


Article

Study on the Influence of Specimen Size and Aggregate Size on the Compressive Strength of Rock-Filled Concrete

Xiang Li ^{1,2}, Yufan Zhang ¹, Tao Yang ^{1,2,*} , Haimei Liao ¹, Lei Yu ¹, Yunke Liu ¹, Guoji Wang ¹, Yinghong Zhao ¹ and Haoyang Qiao ¹

¹ College of Civil Engineering, Guizhou University, Guiyang 550025, China; xli1212@163.com (X.L.)

² Guizhou Provincial Key Laboratory of Rock and Soil Mechanics and Engineering Safety, Guiyang 550025, China

* Correspondence: tyang3@gzu.edu.cn

Abstract: Rock-filled concrete (RFC) technology is a new type of mass concrete construction technology, which consists of two basic components: the force transfer frame formed by large-size rock accumulation and the matrix formed by self-compacting concrete (SCC) filling. Its unique construction method also distinguishes RFC from ordinary concrete in terms of its force characteristics. In this paper, RFC is considered as a composite material consisting of aggregate and SCC; based on the realistic failure process analysis (RFPA) method, the effects of specimen size and aggregate size on the compressive strength of RFC were studied. Firstly, RFC cube specimens were prepared and uniaxial compression tests were conducted. During the preparation process, in order to eliminate the influence of factors such as shape, spatial distribution state, and volume share of aggregates on the compressive strength, aggregates of different sizes were set as spheres and arranged in simple cubic stacking; then a numerical model of RFC with different specimen sizes and different aggregate sizes was established for uniaxial compression numerical simulation experiments to analyze the variation law and failure pattern of the RFC compressive strength. The results indicate that the compressive strength of RFC exhibits a significant size effect and follows a negative exponential function distribution law; with the same volume fraction of aggregate, the smaller the aggregate size, the higher the compressive strength of the RFC will be, and this increasing trend gradually levels off. Based on the findings of this study, it is recommended that the size effect and the reduction of aggregate size on dam strength be taken into account in the design of RFC dams.

Keywords: rocked-filled concrete; compressive strength; aggregate size; size effect



Citation: Li, X.; Zhang, Y.; Yang, T.; Liao, H.; Yu, L.; Liu, Y.; Wang, G.; Zhao, Y.; Qiao, H. Study on the Influence of Specimen Size and Aggregate Size on the Compressive Strength of Rock-Filled Concrete. *Appl. Sci.* **2023**, *13*, 6246. <https://doi.org/10.3390/app13106246>

Academic Editors: Hongyuan Liu, Tao Zhao and Bin Gong

Received: 17 March 2023

Revised: 11 May 2023

Accepted: 17 May 2023

Published: 19 May 2023



Copyright: © 2023 by the authors. Licensee MDPI, Basel, Switzerland. This article is an open access article distributed under the terms and conditions of the Creative Commons Attribution (CC BY) license (<https://creativecommons.org/licenses/by/4.0/>).

1. Introduction

Rock-filled concrete (RFC) technology has been developed based on self-compacting concrete (SCC), which is a mass concrete construction technique. Its construction process includes stacking large-size stones (particle size > 30 cm) in the specified formwork, and then pouring SCC. When pouring SCC, its high fluidity is used to fill the gaps between stones without vibration or rolling process. Compared with ordinary concrete, RFC has the advantages of high construction efficiency, low hydration heat, energy conservation, and environmental protection [1–3]. Due to its excellent performance, RFC has been put into practical engineering application since 2005, and by the end of 2021, there have been 126 RFC dams completed or under construction in China, including 115 gravity dams and 11 arch dams [4].

In a study of RFC material properties, Jin et al. [1] first proposed RFC construction technology, and tested the flow performance of SCC in the rockfill and the compressive strength of RFC. An et al. [5] tested the compactness, compressive strength, tensile strength, and permeability of RFC, indicating that RFC meets the requirements of hydraulic concrete. Liang et al. [6] established the RFC model containing rock, SCC, and interface transition

zone, and tested the elastic modulus of RFC by compression simulation experiments, which put forward the prediction formula of the elastic modulus of RFC in the hardening process based on the Dual Eigenstrain method. He et al. [7] conducted compression creep and shrinkage tests on RFC and SCC, revealing that the creep and shrinkage strains of RFC were lower than those of SCC; additionally, they found that rock aggregates had a significant impact on the creep behavior of RFC. Wei et al. [8] tested the mechanical properties of RFC specimens by coring the borehole of the dam, which showed that the average compressive strength of RFC was slightly greater than the SCC strength, but much less than the rock strength. Li et al. [9] conducted uniaxial compression tests on 39 RFC cube cutting specimens; these cutting specimens were taken from a large volume test block cast in situ using the same material, process, and environment as the construction site. The results of the test showed that the compressive strength of the cutting specimens ranged from 20.7 Mpa to 51.1 Mpa, with a standard deviation of 6.3 Mpa. The strength distribution was quite scattered, which could be attributed to the differences in the size of the aggregate in the specimen, the randomness of the aggregate shape, the randomness of the spatial distribution of the aggregate, and the different proportions of the aggregate in different specimens. The three RFC cutting specimens from the construction site in Figure 1 showed the highly random shapes and spatial distribution of the aggregates. However, it is important to note that the impact of specimen size on the results has not been fully considered in previous studies on the mechanical properties of RFC. Additionally, in practical projects, the aggregate size in RFC is often randomly distributed between 30 cm and 100 cm, and in recent years, some projects have even used aggregate sizes exceeding 100 cm. It is unclear whether the effect of aggregate size on the mechanical properties of RFC is significant or not. Therefore, it is crucial to investigate the impact of both specimen size and aggregate size on the compressive strength of RFC.

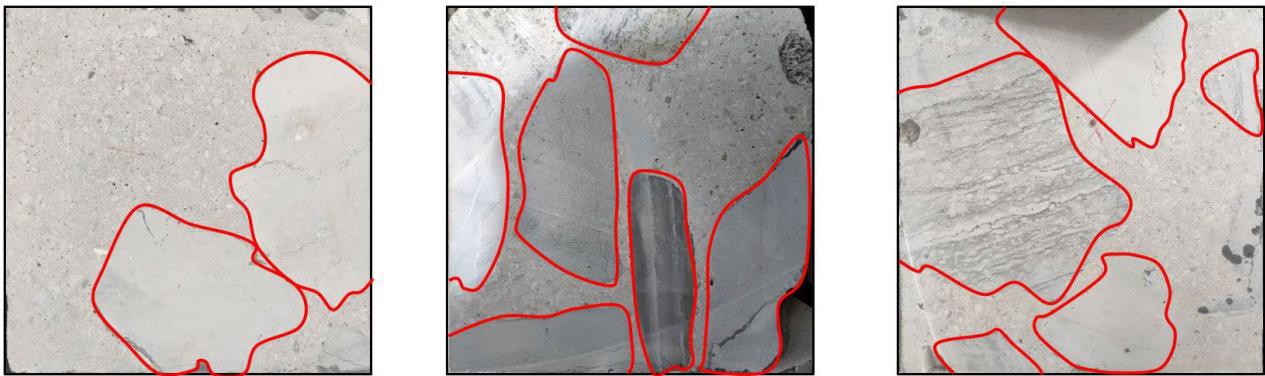


Figure 1. RFC cutting specimen (the red outline indicates the rock aggregate shape).

The strength of quasi-brittle materials, such as rock and concrete, exhibits a size effect, where the strength decreases in a regular manner as the specimen size increases. For concrete, Sim et al. [10] conducted an experiment on lightweight concrete specimens and compared their compressive strength with that of common concrete under different specimen sizes; the results indicated that the size effect of lightweight concrete was more pronounced, and the researchers proposed a prediction formula for the size effect, which takes into account the unit weight of concrete. In a study by Del Viso et al. [11], the compressive strength of high-strength concrete cylinder and cube specimens was analyzed, revealing that the size effect was more significant in cube specimens. Zhuo et al. [12] developed a numerical model for recycled aggregate concrete (RAC) based on microscopic mechanics and investigated the impact of maximum aggregate size (MAS) on the size effect of the compressive strength of RAC; the results showed that an increase in MAS inhibited the size effect.

RFC is composed of rock aggregate and SCC. The force transfer skeleton formed by rock aggregate makes RFC different from ordinary concrete in stress characteristics. For

rock materials, Liu et al. [13] analyzed the uniaxial compressive strength of seven kinds of rocks at different sizes and fitted the strength with a negative exponential function, with good fitting results. Li et al. [14] conducted uniaxial and triaxial compression tests on slate specimens with different diameters, and found that the uniaxial and triaxial compressive strengths of slate exhibit the same size effect law, which was incorporated into the Hoek–Brown and Saeidi failure criteria. Masoumi et al. [15] proposed a constitutive model that considers the influence of rock size on mechanical properties based on the boundary interface plasticity theory, and conducted uniaxial and triaxial compression tests on sandstone specimens with different diameters; the results showed that the model could predict the stress–strain behavior in the experiments well. At present, compared to rock and ordinary concrete, the size effect of RFC still needs to be further studied.

In a study of particle reinforced composites, Lloyd [16] found that the smaller the size of the reinforced particles, the higher the overall strength of the material in the tensile test of aluminum alloy reinforced by 15% silicon carbide particles; on this basis, Yu et al. [17] established a numerical model to reproduce the above experiment and obtained the same conclusion. Wang et al. [18] tested the mechanical properties of silicon carbide particle-reinforced composite materials with two particle diameters, and the results showed that the distribution of the silicon carbide particles with small particle diameters in the matrix was more uniform, and the strength of the composite materials was also higher. Lee [19] studied the relationship between the tensile strength and the particle size of particle-reinforced elastic composite, and found that the tensile strength of the material decreased with the increase in particle size.

For RFC with large-size aggregate as reinforcement, this paper aims to reveal the size effect law of its compressive strength and the influence of aggregate size on its strength. Based on the variation law of the compressive strength of RFC under different specimen sizes and aggregate sizes, this article provides a certain reference basis for the design of RFC dams.

2. Materials and Methods

2.1. Physical Experiment Scheme

In order to avoid the influence of different aggregate shapes, random aggregate spatial distribution, random aggregate strength, and significant difference in aggregate proportions on the compressive strength of each RFC specimen cut on site, this paper assumes that the aggregate shape is spherical, and establishes the ideal model of RFC through simple cubic stacking to form a force transfer skeleton. Firstly, we prepared plastic spherical molds with different diameters whose tops contained a round hole with a diameter of 10 mm to facilitate the insertion of the funnel. Then, C50 strength grade grouting material was poured into the mold through the funnel to form a sphere to simulate rock aggregate (Figure 2a), and the mold was removed after the sphere aggregate acquired its initial strength (Figure 2b). After the mold removal, the sphere aggregate was cleaned of surface dust to prevent the dust from reducing the bonding performance of the aggregate and the SCC; then the aggregate was put into the cube formwork for simple cubic stacking (Figure 2c). Finally, C30 strength grade SCC was poured to fill the empty spaces in the cube mold, and the volume fraction of aggregate was about 52.4% (Figure 2d). The formwork was removed 24 h after the specimen was formed, and it was maintained in the standard curing room for a duration of 28 days. After curing, rock mechanics test (RMT) equipment was utilized to perform a uniaxial compression test on the specimen, and the displacement loading was employed with a loading rate of 0.01 mm/s (Figure 3). In addition, we poured the above C50 strength grade grouting material and C30 strength grade SCC into cubic specimens for strength testing with a side length of 150 mm. The test results showed that the uniaxial compressive strengths of the two were 47.4 Mpa and 29.2 Mpa, respectively, which met the requirements of the strength grade.



Figure 2. RFC specimen-making process. (a) Spherical aggregate is poured; (b) Aggregate demolding; (c) Aggregate accumulation; (d) SCC pouring.

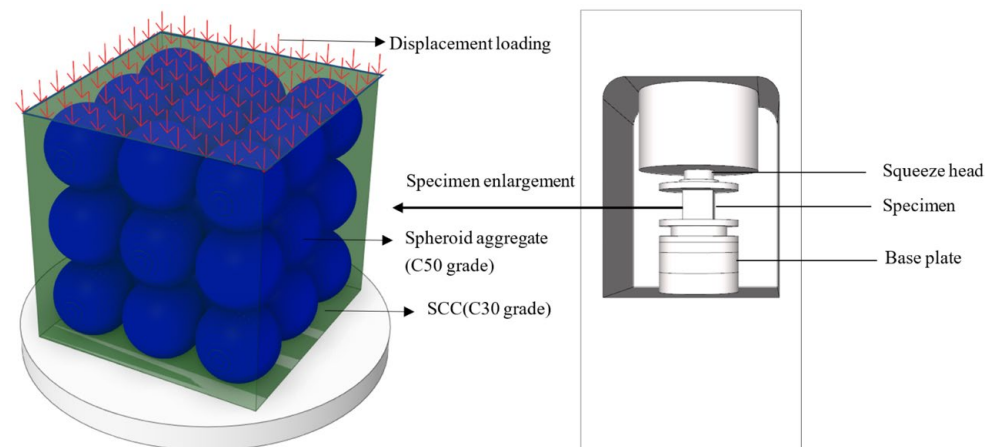


Figure 3. Diagram of unconfined uniaxial loading of specimen.

Three kinds of RFC with different aggregate sizes were designed in the physical experiments. The specimen sizes were 150 mm, and the aggregate sizes were 150 mm, 75 mm, and 50 mm, respectively. The number of aggregates contained in the specimens was 1, 8, and 27, separately (Figure 2c). Limited by the upper pressure limit of the experimental equipment, the larger size of the RFC specimens could not be compressed, so it was difficult to determine the characteristic size of the RFC. Therefore, the purpose of the physical experiment was only to verify the impact of aggregate size on the compressive strength of the RFC, and the study on the effect of specimen size on the mechanical properties of RFC was mainly completed through numerical experiments.

2.2. Principles of Numerical Calculation

Tang [20] proposed the RFPFA method from the perspective of damage mechanics for the nonlinear problem of the rock fracture process. This method considers that each element satisfies the elastic–brittle constitutive relationship at the micro level; the mechanical properties of the set element obey the Weibull distribution, and the stress and strain of the element are calculated by the finite element method, which is a material failure process analysis method for simulating the mechanical problems of a discontinuous medium through the continuous medium mechanics method. The Weibull distribution probability density function of material parameters is as follows:

$$\varphi(\alpha) = \frac{m}{\alpha_0} \cdot \left(\frac{\alpha}{\alpha_0}\right)^{m-1} \cdot e^{-\left(\frac{\alpha}{\alpha_0}\right)^m} \quad (1)$$

where α represents the mechanical property parameter of the material element; α_0 is the average value of the mechanical property parameters of the element; m is the property parameter of the distribution function, and its physical meaning reflects the homogeneity of the material; and $\varphi(\alpha)$ represents the probability density of the mechanical properties of the material elements.

Each element in the RFPA follows the Mohr–Coulomb strength criterion, and its shear damage envelope surface under three-dimensional conditions is as follows:

$$F = \frac{f_c}{\frac{\varepsilon_1}{1+\mu} + \frac{\mu}{(1+\mu)(1-2\mu)}\varepsilon_v - \left[\frac{\varepsilon_3}{1+\mu} + \frac{\mu}{(1+\mu)(1-2\mu)}\varepsilon_v \right] \frac{1+\sin\phi}{1-\sin\phi}} \tag{2}$$

Its tensile damage envelope is as follows:

$$F = \frac{-f_t}{\frac{\varepsilon_1}{1+\mu} + \frac{\mu}{(1+\mu)(1-2\mu)}\varepsilon_v} \tag{3}$$

where μ represents Poisson’s ratio; f_c represents uniaxial compressive strength; f_t represents uniaxial tensile strength; $\varepsilon_1, \varepsilon_2,$ and ε_3 represent the three principal strains; ε_v represents the volumetric strain; and ϕ represents the internal friction angle.

The strain energy of the element follows the formula [21]:

$$U^e = \frac{1}{2E} \left[\sigma_1^2 + \sigma_2^2 + \sigma_3^2 - 2\nu(\sigma_1\sigma_2 + \sigma_2\sigma_3 + \sigma_1\sigma_3) \right] \tag{4}$$

where U^e is the strain energy of the element; E is the elastic modulus of the element; and $\sigma_1, \sigma_2, \sigma_3$ are the three principal stresses.

Yang [22] refined the damage path of the RFPA method on the basis of Tang [20], extending it to multi-path damage analysis. First, the five basic states of the element are defined: elasticity, tensile failure, compressive failure, tensile separation, and compressive contact (Figure 4). The element state of the current step is determined by three factors: the current step’s stress–strain level, the previous step’s material parameters, and the element damage history. Then, 25 load–damage paths are extended for elements with different damage states; for example, the element that has been damaged by tension is closed again under pressure, and the element that has been damaged by compression is opened again under tension. Finally, the constitutive relationship is determined according to the element state and damage path, and the material parameters of the current step’s element can be calculated by substituting the initial material parameters. On the basis of the RFPA and multi-path damage analysis method, Yang [23] developed the rock engineering analysis system, and obtained the law of size effect of rock permeability by using the system to simulate the fracture process of rock under stress–seepage field coupling. The numerical simulation in this study is implemented by this rock engineering analysis system.

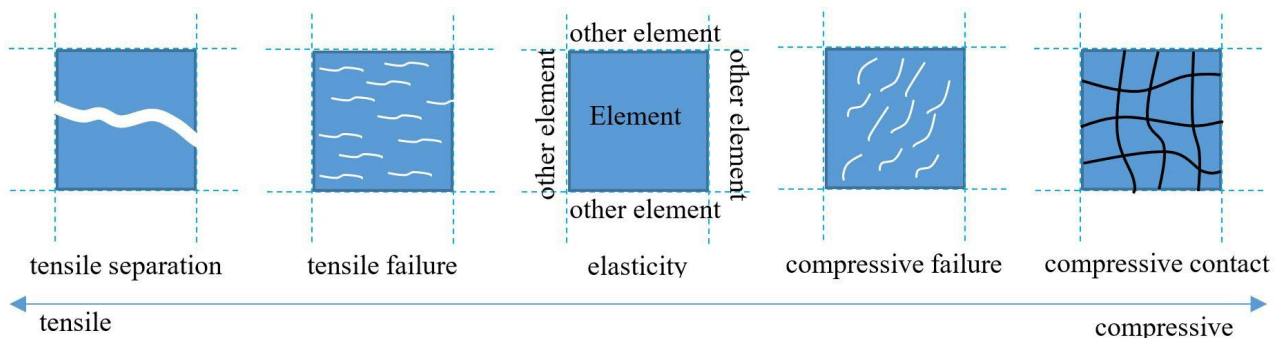


Figure 4. Schematic diagram of element status [22].

2.3. Numerical Simulation Experiment Scheme

The numerical experiment set the aggregate as a circle, and the RFC numerical model with different sizes was established by increasing the number of elements while keeping the element size of 10 mm unchanged. The shape of the model was square, with sizes ranging from 150 mm to 3000 mm. A numerical model was established every 150 mm, and five types of aggregate sizes were set: type 1 to type 5 (Figure 5b). The numerical model was named “specimen size—particle size type”. Here, the particle size type was defined as the variable t , whose physical meaning was the number of circular aggregates in the direction of the model side length; specimen size was the variable l (mm); and aggregate size was the variable r (mm), where $r = l/t$. When the specimen size was unchanged, it could be seen that the aggregate size was inversely proportional to the particle size type. In Figure 5b, the longitudinal direction represents the increase in specimen size, and the transverse direction represents the increase in particle size type, i.e., the decrease in aggregate size. The SCC model and the rock model corresponding to RFC, respectively, is shown in Figure 5a,c. Because the mechanical properties of each element follow Weibull random distribution, even with the same numerical model, its calculation results often have small differences. Therefore, this study carried out three numerical calculations with the same parameters for each model, and took its average value as the basis for judging the uniaxial compressive strength, with a total of 420 numerical experiments. The corresponding numerical model names of the RFC specimens with three aggregate sizes (150 mm, 75 mm, 50 mm) in Section 2.1 are “150-type1, 150-type2, 150-type3”.

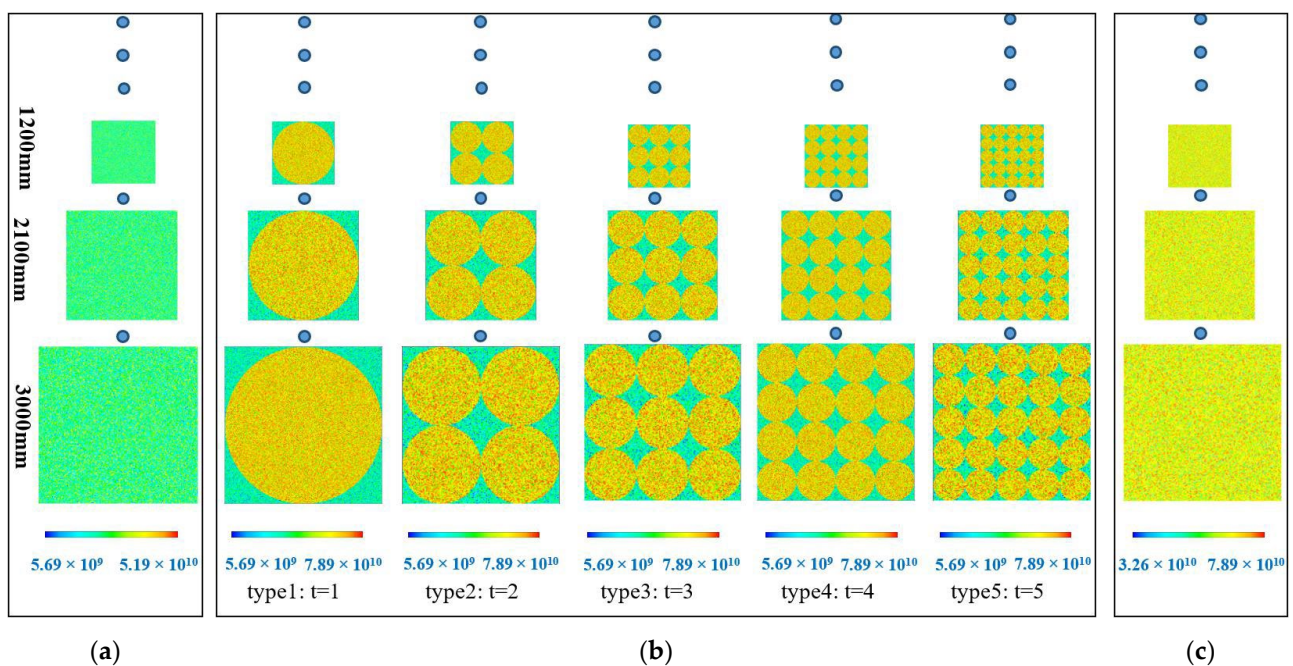


Figure 5. Numerical experiment design scheme (elastic modulus nephogram, unit: Pa). (a) SCC model; (b) RFC model; (c) Rock model.

3. Results

3.1. Effect of Specimen Size on Compressive Strength

Regarding the results of the numerical simulation experiment, RFC with specimen sizes of 600 mm, 1200 mm, 1800 mm, 2400 mm, and 3000 mm for each particle size type was selected to analyze the failure mode (Figure 6). For RFC of type 1, cracks around the aggregate appeared in all models, and through-cracks appeared in the aggregate in the 1200 mm and 3000 mm specimen size models. For RFC of type 2, there were individual aggregates destroyed in all models. For RFC of type 3 to type 5, there was no obvious law between specimen size and failure mode; in most models, multiple aggregates were

damaged and inclined through-cracks were formed. Overall, as the particle size type increased, i.e., the size of the aggregate decreased, the crack extension area of the RFC gradually shifted from the interface to the aggregate, and as the main crack extended, the quantity of smaller cracks increased and their distribution became more widespread. This was due to the hindrance of coarse aggregate in the transfer of internal force and the expansion of internal cracks in the concrete under static uniaxial compression load; this barrier becomes more pronounced with increasing aggregate size [24]. When the proportion of aggregates is the same, the RFC model containing large-sized aggregates has poor overall deformation coordination ability, and the larger aggregates prevent the initial crack from expanding, causing most cracks to bypass the larger aggregate particles and expand around the weak interface zone.

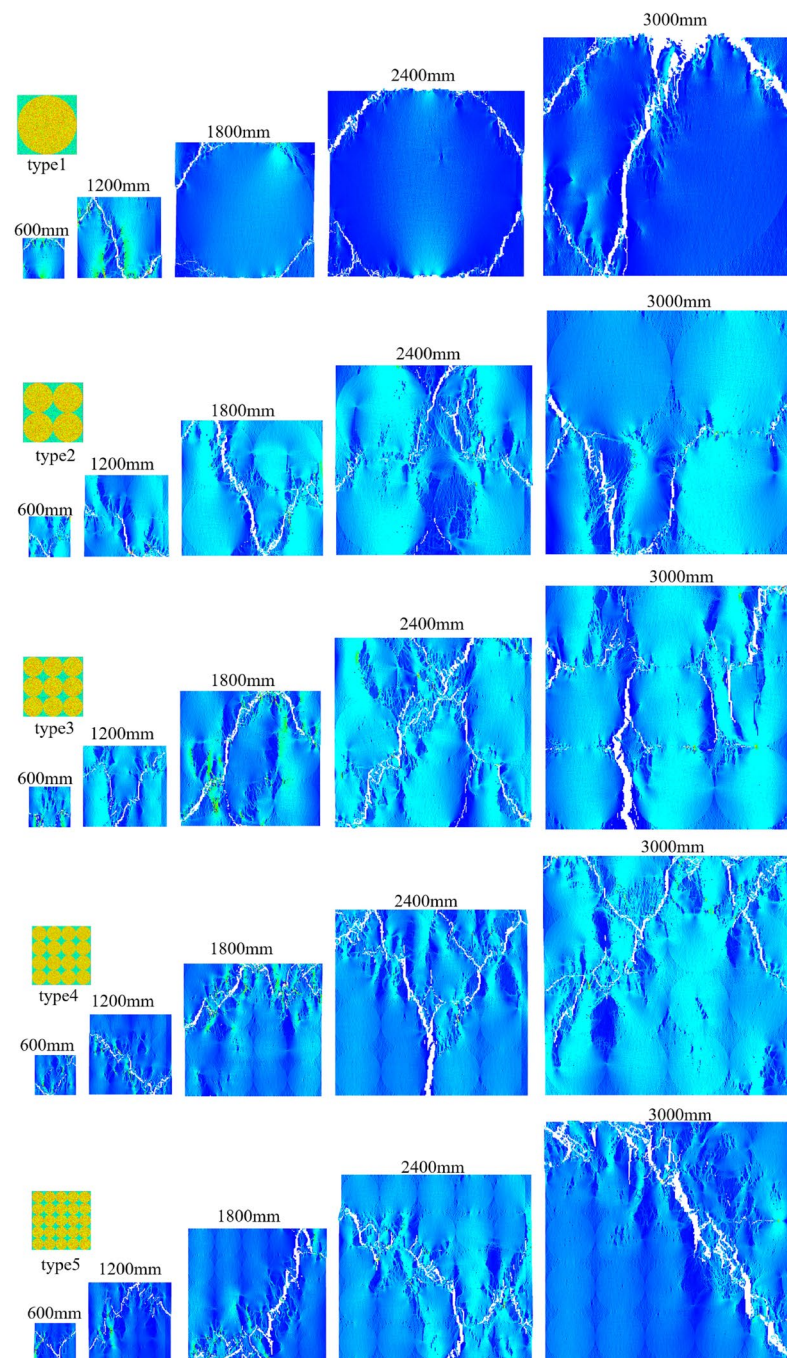


Figure 6. Failure modes of RFC with different specimen sizes (shear stress nephogram).

We compared the stress–strain relationship of RFC with different specimen sizes (600 mm, 1200 mm, 1800 mm, 2400 mm, 3000 mm) under each particle size type (Figure 7). As can be seen, the compressive strength of RFC has an obvious size effect under each particle size type. However, with the increase in specimen size, there is no significant change in the modulus of elasticity of RFC.

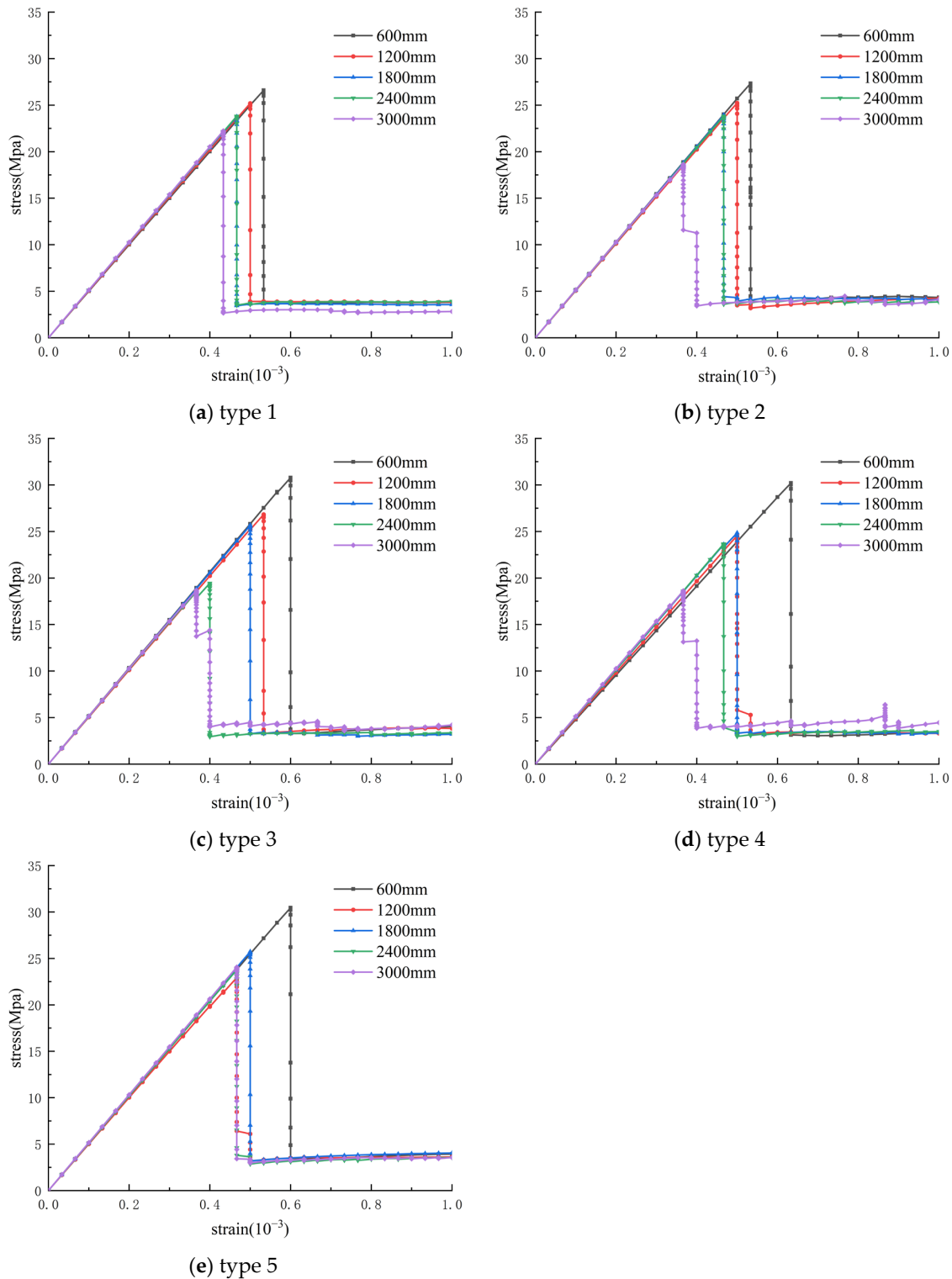


Figure 7. Constitutive relation curves of RFC under different specimen sizes.

The uniaxial compressive strength data for the three materials, SCC, RFC of each particle size type, and rock, are shown in Table 1, and the resulting data were fitted by using the negative exponential function fitting form:

$$f_c(l) = a + be^{-cl} \tag{5}$$

where l is the specimen size; $f_c(l)$ is the corresponding compressive strength; and a , b , and c are the fitting undetermined parameters.

Table 1. Compressive strength of three materials (unit: Mpa).

Size (mm)	SCC	Type1	Type2	Type3	Type4	Type5	Rock
150	24.07	33.50	36.30	38.63	33.27	34.67	46.33
300	24.23	31.60	30.17	34.70	31.40	34.17	44.20
450	22.53	30.40	30.17	33.63	30.80	34.53	44.13
600	22.80	28.30	28.90	30.20	29.07	31.27	43.03
750	19.50	27.23	27.67	29.70	26.83	29.80	41.73
900	19.60	25.73	29.07	28.03	27.30	27.23	41.03
1050	19.17	25.37	27.27	26.83	27.03	27.97	37.43
1200	20.17	24.67	24.70	24.50	26.73	25.40	40.33
1350	20.17	24.60	25.67	25.73	26.87	28.57	38.97
1500	18.10	23.70	25.07	25.43	25.23	26.30	37.47
1650	19.63	22.67	25.63	25.10	25.30	26.97	38.23
1800	17.77	22.63	23.93	24.57	25.70	24.63	34.13
1950	18.13	23.83	24.53	23.40	24.33	25.13	35.80
2100	17.53	22.03	23.93	25.67	24.93	24.87	38.30
2250	17.50	23.83	23.57	21.60	23.90	24.57	34.87
2400	15.03	22.67	23.23	21.20	21.93	23.10	37.60
2550	17.87	22.77	21.67	24.00	23.90	24.00	34.87
2700	14.77	22.20	21.17	24.00	23.37	22.20	34.87
2850	16.43	22.20	22.27	22.23	23.40	24.60	34.87
3000	16.17	22.23	20.40	21.10	22.30	24.03	33.47

The undetermined parameters in Table 2 were obtained by fitting, and the fitting curves of the compressive strength under different specimen sizes were obtained (Figure 8). It can be seen that the three materials have significant size effect. With the increase in specimen size, the compressive strength of the three materials gradually decreased, and the decreasing trend was gradually flat, indicating that RFC, SCC, and rock had the same size effect law. When the size of the specimen was greater than a critical value, there was no obvious change in the strength. This critical value is called the characteristic size of the material strength. The slope of the fitting curve could be obtained by differentiating the fitting function:

$$f_c'(l) = -cbe^{-cl} \tag{6}$$

Table 2. Fitting parameters of size effect.

Fitting Parameter	SCC	Type 1	Type 2	Type 3	Type 4	Type 5	Rock
a	14.08	22.08	20.37	22.20	22.06	22.62	32.76
b	11.11	14.50	15.06	19.64	12.17	15.09	15.03
c	5.89×10^{-4}	1.41×10^{-3}	7.95×10^{-4}	1.34×10^{-3}	8.52×10^{-4}	9.64×10^{-4}	7.21×10^{-4}
characteristic size (mm)	8275	4265	6891	4676	6261	5885	7460

Here, the corresponding l value when the curve slope is -0.005% is taken as the characteristic size of the material (Table 2). There is no obvious law between the particle size type and the characteristic size.

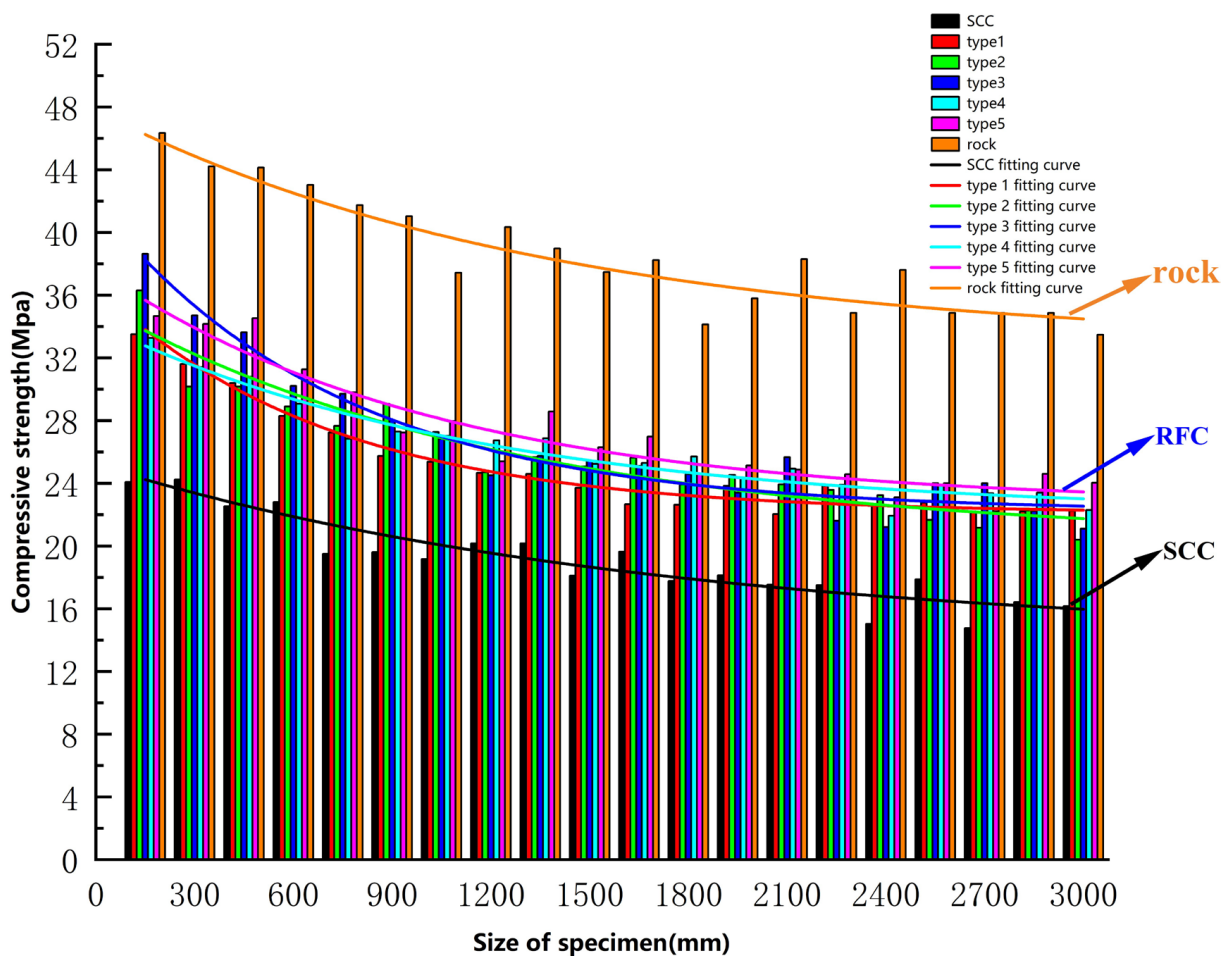


Figure 8. The fitting curve of size effect of compressive strength.

3.2. Effect of Aggregate Size on Compressive Strength

This study validates the reliability of the numerical experiments by comparing the failure pattern of RFC in the physical and numerical experiments. Figure 9a,b illustrate the damage state of the specimen surface and internal aggregate in the physical experiment, respectively, and Figure 9c shows the corresponding numerical simulation experiment of the RFC. The failure modes of RFC could be divided into interfacial failure and splitting aggregate failure as a whole. For RFC with aggregate size of 150 mm, there were obvious through-cracks in aggregates (marked as A1 and A2) in both the physical and numerical experiments due to the single aggregate being the main body under stress, and the failure mode of the specimens was splitting failure. For RFC with aggregate size of 75 mm, vertical cracks along the interface appeared on the surface of the specimen, and inclined cracks occurred when the aggregate at the B1 mark was destroyed; the aggregate splitting failure at the B2 mark corresponded to the inclined cracks at the B1 mark; the aggregate failure at mark B3 corresponded to that at marks B1 and B2. For RFC with aggregate size of 50 mm, a large amount of the SCC on the surface of the specimen fell off, exposing the internal aggregate; the aggregate at the mark C1 exhibited extrusion phenomena due to the failure of the interface, and the aggregate at the mark D1 exhibited splitting failure; cracks distributed around the aggregate at the C2 mark corresponded to the C1 mark, and inclined cracks through the aggregate at the D2 mark corresponded to the D1 mark. The RFC failure modes of the three aggregate sizes were well compared in the physical experiment and the numerical experiment, which indicated the reliability of the numerical experiment.

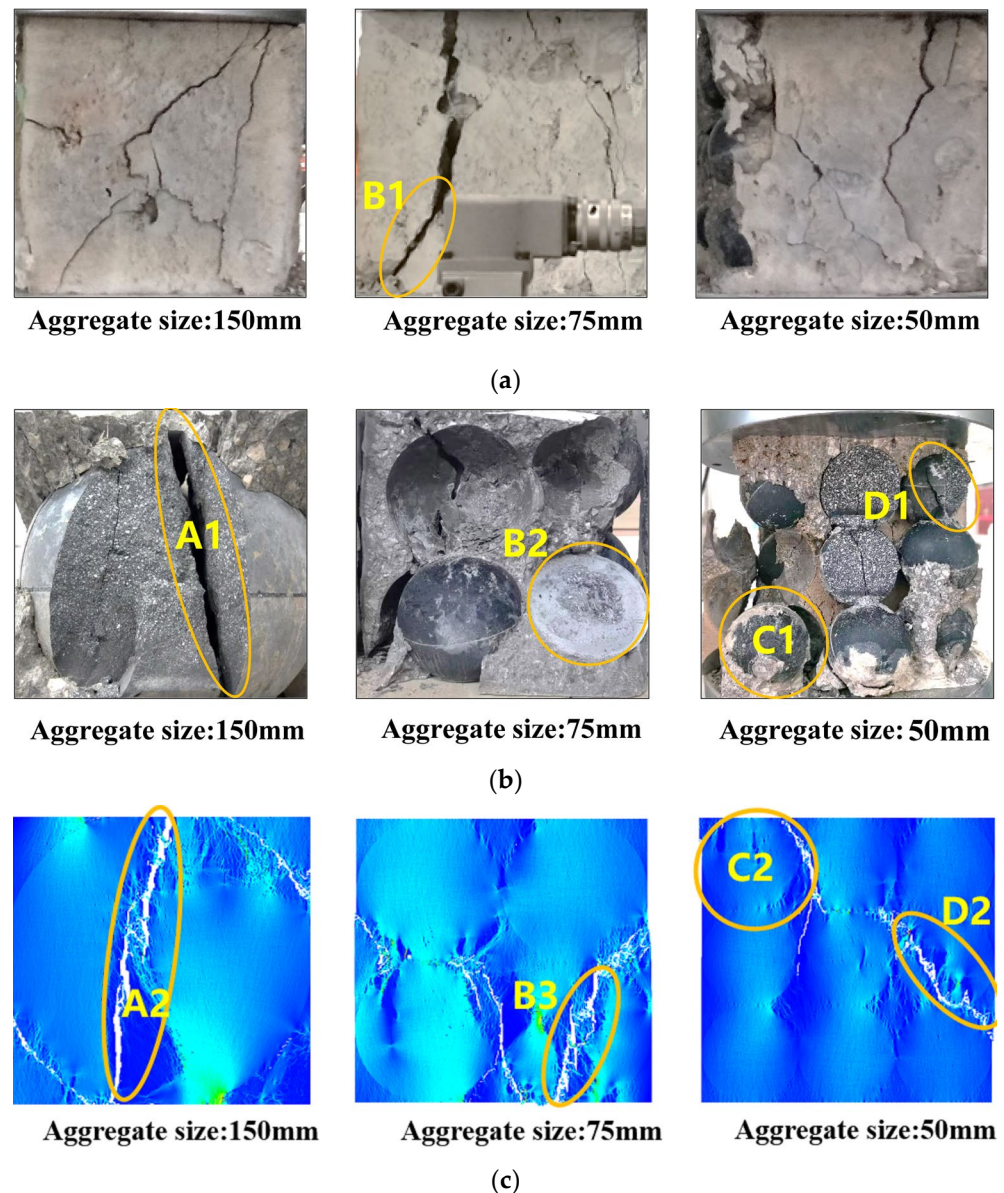


Figure 9. Failure mode of RFC with different aggregate sizes. (a) Failure mode of specimen surface (front); (b) Failure mode of internal aggregate (left side); (c) Failure mode of numerical model (shear stress nephogram).

RFC numerical models with aggregate sizes of 3000 mm, 1000 mm, and 600 mm, respectively, were selected to reproduce the process of RFC from micro-element damage to micro-crack development and finally to macro-crack formation (Figure 10). The red color represented tensile damage elements, and the green color represented shear damage elements. For RFC with aggregate size of 3000 mm, when the load was close to the peak strength (strain of 0.43×10^{-3}), a large number of tensile damage elements developed along the interface, forming cracks distributed around the aggregate (marked as A); when the loading strain reached 0.47×10^{-3} , it entered the post-peak softening stage, and the cracks at mark A continued to develop along the edge of the aggregates, and the elements inside the aggregates underwent tensile damage; when the loading strain reached 0.67×10^{-3} , due to the further expansion of the interface cracks, the SCC stopped working, and as the main body bearing the load, the internal damage elements of the aggregates gradually increased, resulting in the appearance of micro-cracks (marked as B); when the loading strain reached 1.00×10^{-3} , the micro-cracks at point B extended into inclined

cracks that penetrated the aggregates (marked as C), and the failure mode of the RFC was similar to that of Brazilian splitting failure.

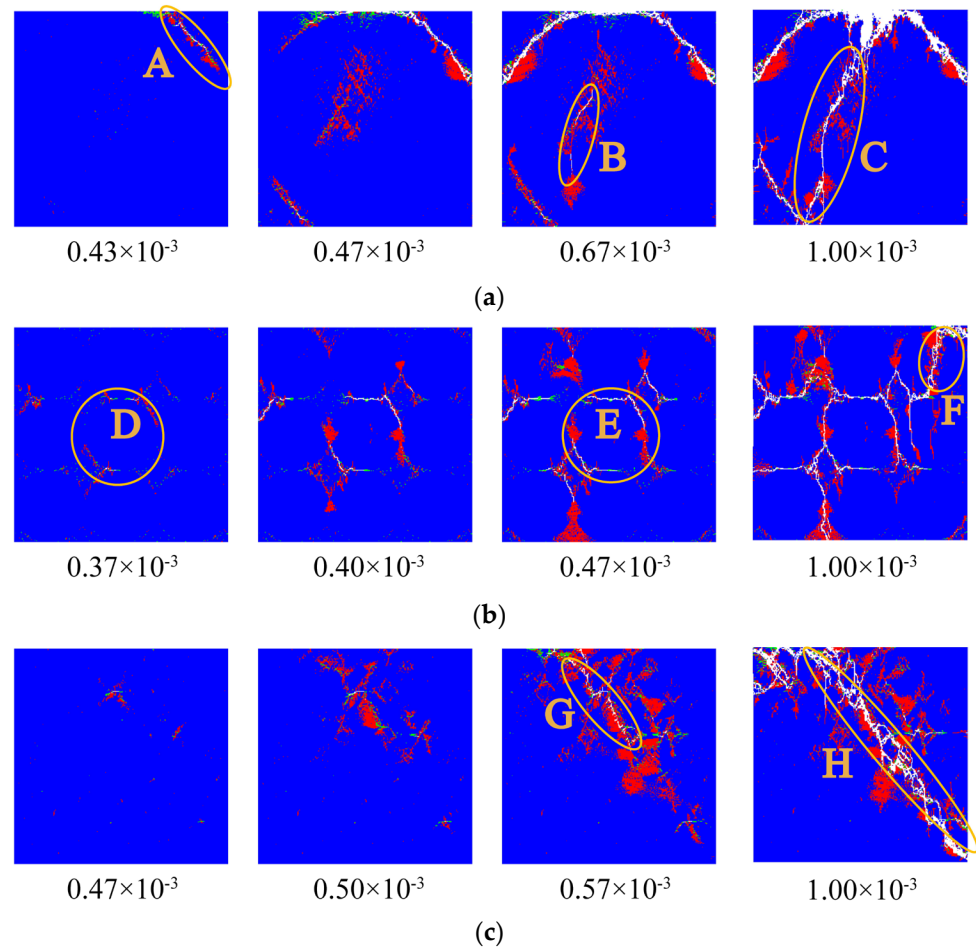


Figure 10. Crack formation process of RFC with different aggregate sizes. (a) Type 1 (aggregate size: 3000 mm), (b) Type 3 (aggregate size: 1000 mm), (c) Type 5 (aggregate size: 600 mm).

For RFC with aggregate size of 1000 mm, when the load was close to the peak strength (strain of 0.37×10^{-3}), a large number of tensile damage elements developed around the edge of the aggregates, forming micro-cracks (marked as D); during the strain range from 0.40×10^{-3} to 1.00×10^{-3} , the tensile damage elements around the aggregates increased, and the micro-cracks expanded into macroscopic cracks distributed around the aggregate (marked as E); when the strain reached 1.00×10^{-3} , the SCC no longer bore the load, causing some aggregates to develop through-cracks (marked as F), and the overall failure mode of the RFC was similar to splitting tensile failure. For RFC with aggregate size of 600 mm, due to the relatively uniform distribution of aggregates, their damage elements did not surround the distribution of aggregates, and with the increase in load, tensile damage elements gradually developed, forming inclined micro-cracks at a strain of 0.57×10^{-3} (marked as G); when the loading strain reached 1.00×10^{-3} , the micro-cracks expanded into inclined cracks that penetrated the specimen (marked as H), and the RFC was characterized by macroscopic shear failure composed of a large number of tensile damaged elements.

As shown in Table 1, this paper used the particle size type as the independent variable to carry out linear fitting on the compressive strength, and the fitting parameters are shown in Table 3. Figure 11 describes some fitting straight lines (the sizes of specimens are 600 mm, 1200 mm, 1800 mm, 2400 mm, and 3000 mm, respectively). The slope of the fitting straight line in Table 3 is positive except for the specimens with sizes of 150 mm and 2400 mm. It

is clear that, on the whole, with the increase in particle size type, that is, the decrease in aggregate size, the compressive strength of RFC gradually increases.

Table 3. Linear fitting parameter of particle size type against compressive strength.

Specimen Size (mm)	Intercept	Slope
150	35.48	−0.07
300	30.50	0.64
450	29.24	0.89
600	27.72	0.61
750	26.96	0.43
900	27.10	0.12
1050	25.40	0.50
1200	24.15	0.35
1350	23.55	0.91
1500	23.54	0.54
1650	22.65	0.83
1800	22.56	0.58
1950	23.53	0.24
2100	22.29	0.67
2250	22.95	0.18
2400	22.56	−0.04
2550	21.86	0.47
2700	21.93	0.22
2850	21.16	0.59
3000	20.36	0.55

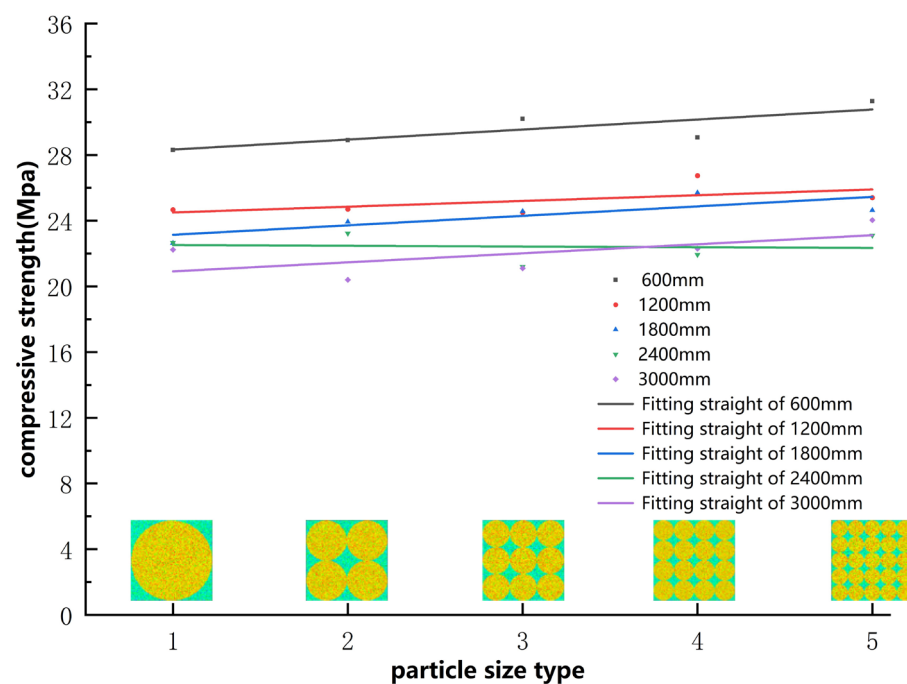


Figure 11. Linear fitting of particle size type to compressive strength.

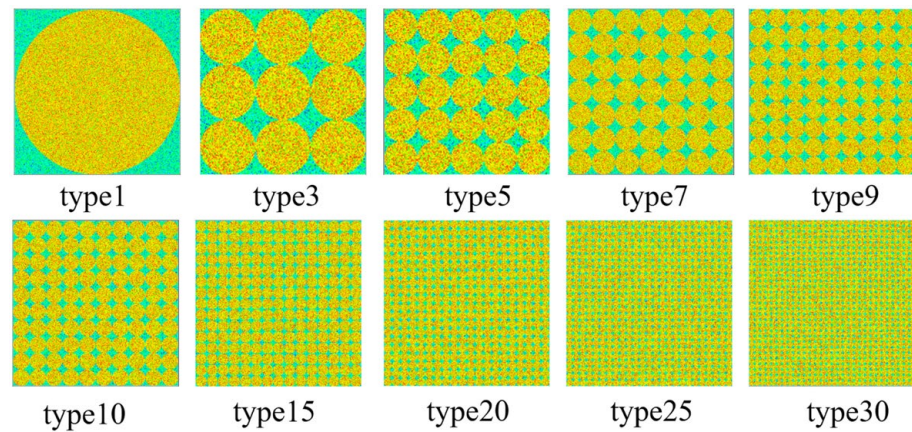
Further Study on the Effect of Aggregate Size on Compressive Strength

As there are only five points of data in the above fit on the compressive strength by particle size type, the fitted straight line contradicts the reality. In practical terms, the compressive strength of RFC cannot increase indefinitely with increasing particle size type, and its maximum value cannot exceed the compressive strength of the aggregate. In order to further investigate the relationship between aggregate size and compressive strength, the size of the numerical model was fixed at 3000 mm in this paper, and more particle size

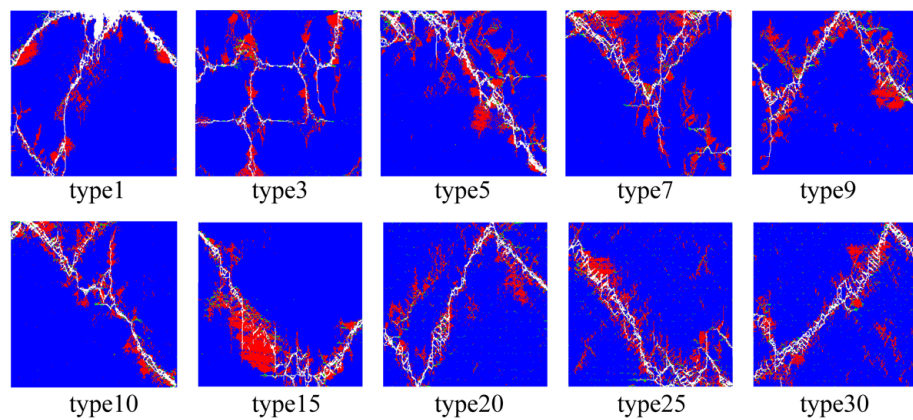
types were added on the basis of the previous ones. The aggregate size and compressive strength corresponding to RFC of each particle size type are shown in Table 4, and some models are shown in Figure 12a.

Table 4. Aggregate size and compressive strength of different types of RFC.

Particle Size Type	1	2	3	4	5	6	7	8	9	10	15	20	25	30
Aggregate size (mm)	3000	1500	1000	750	600	500	428	375	333	300	200	150	120	100
compressive strength (Mpa)	22.23	20.40	21.10	22.30	24.03	23.43	22.87	24.63	24.10	24.60	24.17	25.80	25.93	27.03



(a)



(b)

Figure 12. Numerical model and element damage nephogram of type 6 to type 30 RFC. (a) Numerical model; (b) Element damage nephogram.

Figure 12b illustrates the post-failure element damage state of RFC of partial particle size types. For type 1 and type 3 RFC with larger aggregate size, cracks mainly developed along the interface, and aggregate failure occurred after the SCC stopped working. For type 5 to type 30 RFC with smaller aggregate size and more uniform distribution, inclined cracks penetrating the specimen occurred after failure, indicating shear failure.

In the numerical simulation experiment of RFC, the strain energy in the element was released in the form of acoustic emission. Figure 13a expresses the relationship between particle size type on acoustic emission and compressive strength. From the close trend of the turning points of the two lines, it can be seen that there is a good correspondence between the total energy released by the acoustic emission and the compressive strength,

that is, the higher the total energy released by acoustic emission, the greater the compressive strength. Figure 13b is a fitting of the data in Figure 13a, and its fitting function is as follows:

$$\begin{aligned} f_c(t) &= 27.07 - 6.38 \times e^{-0.08t} \\ E(t) &= 16.07 - 7.51 \times e^{-0.07t} \end{aligned} \tag{7}$$

where t is the particle size type; $f_c(t)$ is the corresponding compressive strength; and $E(t)$ is the total energy released by the corresponding acoustic emission.

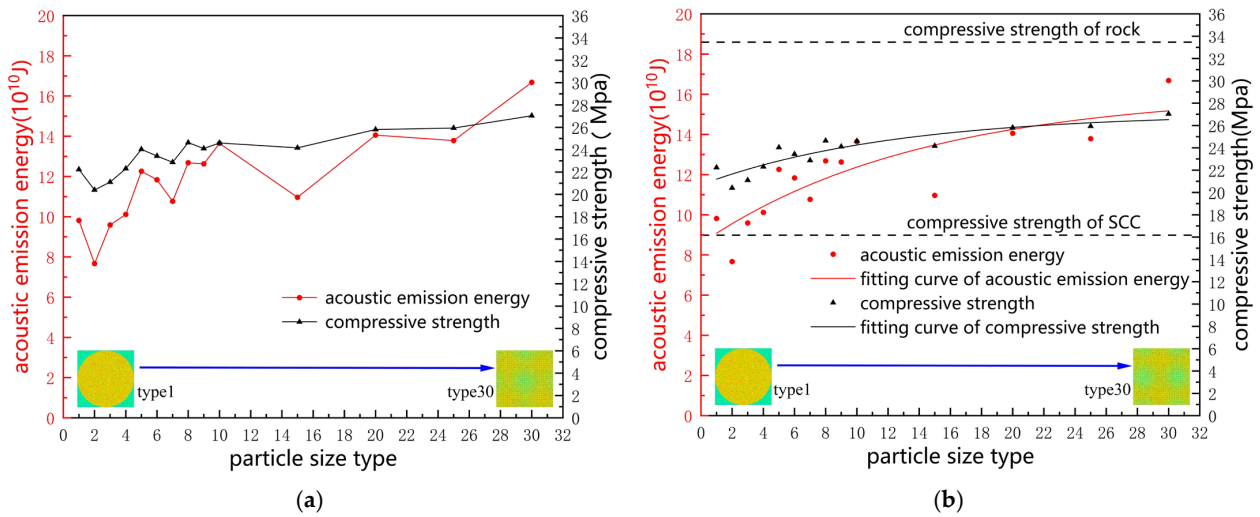


Figure 13. Effect of particle size type on compressive strength and acoustic emission energy. (a) Compressive strength and acoustic emission energy; (b) Fitting curve.

The two dashed lines in Figure 13b represent the compressive strength of SCC and rock under the same specimen size (3000 mm). The strength of RFC with each particle size type is distributed between the strength of rock and SCC. From the fitted curve of compressive strength, it shows that, while keeping the proportion of aggregate unchanged, the compressive strength of RFC gradually increases with the increase in particle size type, i.e., the decrease in aggregate size, and the increasing trend gradually tends to flatten, with a maximum compressive strength of 27.07 Mpa.

3.3. Influence of Dual Factors of Specimen Size and Aggregate Size on Compressive Strength

In this section, specimen size and particle size type were taken as variables to fit the compressive strength of RFC. By referring to Formula (5) and Formula (7), the fitting surface function was set as a negative exponential function of bivariable, and the fitting function was written as follows:

$$f(l, t) = 24.86 + 15e^{-0.0011l} - 4.38e^{-0.1t} \tag{8}$$

where l is the specimen size, t is the particle size type, (d/t) is the aggregate size, and $f(l, t)$ is the corresponding compressive strength.

The fitting surface is shown in Figure 14, where the red balls represent the compressive strength of RFC in Table 1. From the perspective of the specimen size direction in Figure 14 (arrow A), the difference between the maximum and minimum compressive strength values of each RFC particle size type is greater than 11 Mpa. However, from the perspective of the particle size type direction (arrow B), the difference between the maximum and minimum compressive strength values of each specimen size RFC is distributed between 1.73 Mpa and 5.36 Mpa. This indicates that the influence of specimen size on compressive strength is more significant relative to aggregate particle size.

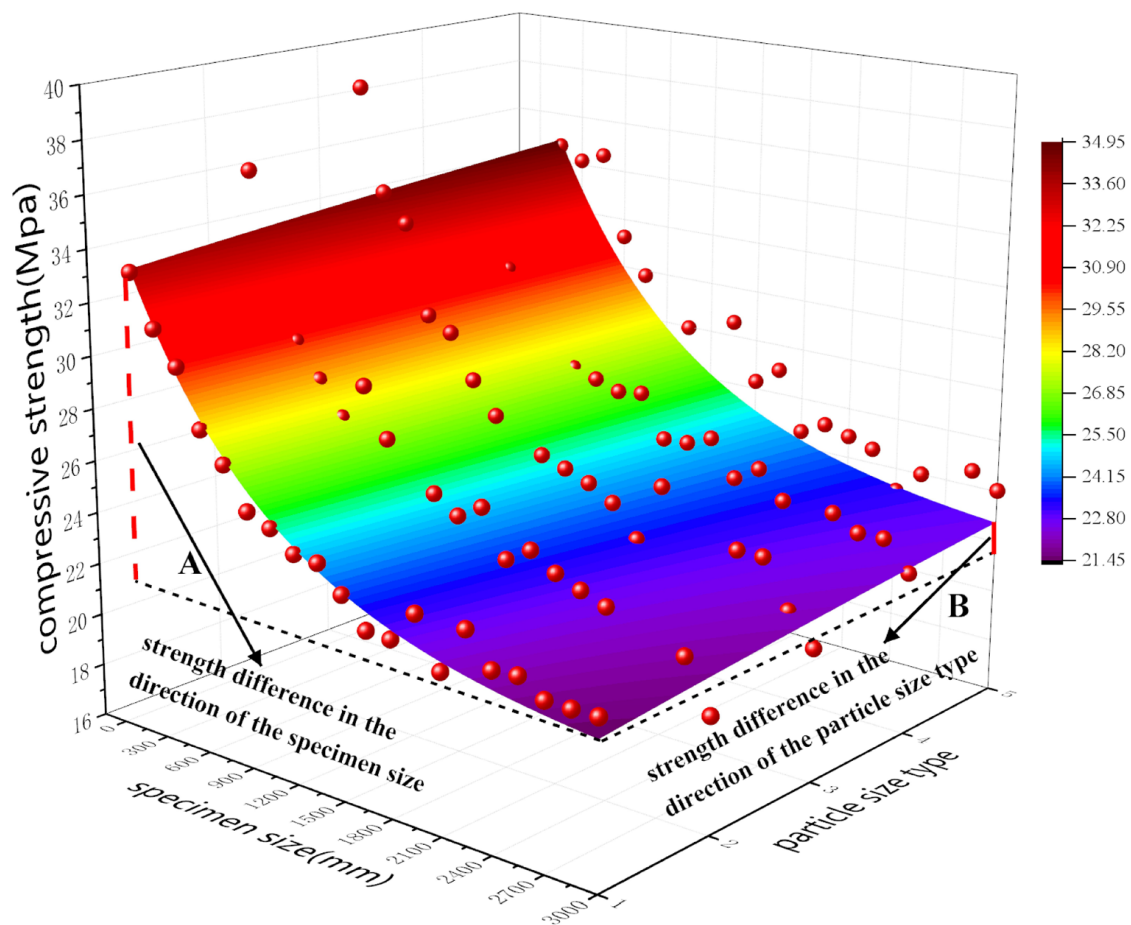


Figure 14. Fitting surface of particle size type and specimen size to compressive strength.

4. Discussion of the Results

To address the phenomenon of the size effect of materials, Weibull [25] put forward a statistical size effect theory based on the weakest chain assumption. It is believed that materials are composed of several basic elements, which are independent of each other and have randomly distributed mechanical properties. The macroscopic strength of a material is determined by the elements with the lowest internal strength, and when the size of the structure increases, the probability of low strength elements inside the material increases, which leads to a decrease in the macroscopic strength of the material. When the size of the structure increases, the probability of low strength elements inside the material increases, which leads to a decrease in the macroscopic strength of the material. The mechanical properties of the elements of the RFPA method obey the Weibull distribution; therefore, in a simulation experiment of quasi-brittle materials, the RFPA method can be used to obtain a more realistic size effect law. Tang et al. [26] first used RFPA to simulate uniaxial compression tests on rock models of different sizes, and the compressive strength showed a significant size effect, which satisfied the negative exponential function law. Liang et al. [27] studied the effects of material homogeneity, confining pressure, and joint density on the size of rock mass, and the results showed that the characteristic size of rock mass decreased with the increase in homogeneity and joint density, and the characteristic strength increased with the increase in confining pressure. Hu et al. [28] investigated the influence of parallel joint spacing on the size effect and characteristic size of rock masses based on the RFPA method, which showed that the characteristic size of the compressive strength increased with the increase in spacing with joints, and produced the negative exponential function equation of the compressive strength of rock masses with specimen size at each joint spacing. Based on the above research conclusions, this article uses the RFPA method to

simulate the uniaxial compression of RFC, and the size effect law of RFC obtained satisfies the negative exponential function, which is reasonable.

In the study of the effect of aggregate size on the compressive strength of concrete, Wu et al. [29] prepared three kinds of aggregate size ranges of concrete cubic specimens; the aggregate size ranges were 5–10 mm, 10–16 mm, 16–20 mm, and the uniaxial compression test of the specimen showed that the compressive strength of concrete increased first and then decreased with the increase in aggregate size. Li et al. [30] used pebbles as coarse aggregates to prepare concrete specimens with four different aggregate size ranges for uniaxial compression testing; the aggregate size ranges were 5–10 mm, 5–20 mm, 5–40 mm, and 5–60 mm, respectively, and the tests showed that as the MAS increased, the compressive strength of the specimens decreased. Jin et al. [31] established a numerical model of concrete containing four different aggregate size ranges, with aggregate size ranges of 5–24 mm, 5–30 mm, 5–36 mm, and 5–42 mm, and investigated the effects of specimen size and MAS on compressive strength through uniaxial compression simulation experiments; the test results showed that the increase in MAS led to a decrease in compressive strength of concrete and made the size effect more significant. Hu et al. [32] used corundum balls to replace coarse aggregate in concrete and prepared cylindrical specimens containing three aggregate sizes for uniaxial compression experiments with aggregate sizes of 3 mm, 6 mm, and 9 mm, and the results showed that with the decrease in corundum ball particle size, the compressive strength of concrete showed an increasing trend.

The reason for the increase in compressive strength with a decrease in aggregate size in the RFC is that the smaller aggregate sizes are more evenly distributed and form a relatively dense fine structure, in the condition of the same percentage of aggregates. When an external load is applied, the smaller the aggregate size is, the stronger the overall deformation coordination ability of the stressed section of the specimen will be, which slows down the specimen damage caused by stress concentration.

Regarding the physical experiments, the compressive strength of the RFC with aggregate size of 150 mm was higher than that of the RFC with aggregate sizes of 75 mm and 50 mm. This was because during the process of aggregate stacking, simple cubic stacking could only be formed by relying on the side support of the mold, which was different from the stable rockfill body in actual engineering (which does not require template support). Additionally, during the casting of SCC, no thick protective layer was set on the edge of the spherical aggregates. During the loading process, the SCC at the corners of the RFC with 150 mm aggregate size was prone to failure first, and then the aggregates bore the main load, resulting in a higher strength. For RFC with aggregate sizes of 75 mm and 50 mm, surface cracks occurred during the loading process, causing the position of the aggregates to shift, and then some spherical aggregates were squeezed out, which led to the instability of the load transfer skeleton and a lower compressive strength. In the subsequent study of how aggregate size affects the mechanical properties of RFC, the thickness of the protective layer on the edge of the aggregates could be increased to prevent the aforementioned phenomena.

5. Conclusions

In this paper, specimen size and aggregate size were considered as variables to study their effects on the compressive strength of RFC, and corresponding numerical experiments were established based on the RFPA method and the multiple path damage analysis method. The failure mode and compressive strength data of RFC were analyzed, and the conclusions are summarized as follows:

- (1) RFC has a formally consistent compressive strength size effect law with SCC and rock, and a better result is obtained by fitting using the negative exponential function. Based on the fitting function, the characteristic sizes of RFC under different particle size types are given in this paper. There is no obvious law between the characteristic sizes and particle size types. The influence of specimen size on the failure mode of RFC is not significant.

- (2) For RFC with the same proportion of aggregate, as the aggregate size decreases, the compressive strength increases, and this increasing trend gradually slows down. The compressive strength of RFC is positively correlated with the total energy released through acoustic emission. RFC with smaller aggregate sizes all exhibit inclined through-cracks after failure, which manifests as a macroscopic shear failure consisting of a large number of tensile damaged elements.
- (3) This paper analyzes the compressive strength data of RFC, and obtains the fitting surface function of specimen size and aggregate size against compressive strength. Based on the fitted surface, it is evident that the effect of specimen size on compressive strength is more pronounced than that of aggregate size.

It should be noted that in this paper, the aggregate in the RFC is simplified as circular and arranged in simple cubic stacking, which is different from actual engineering situations. In practical engineering, the mechanical properties of RFC vary greatly due to the irregular shape of rock and the randomness of its spatial distribution. Based on this paper, further research can be conducted to investigate the impact of the coupling of these complex factors on the compressive strength of RFC.

Author Contributions: Conceptualization, X.L.; methodology, T.Y. and X.L.; software, T.Y.; validation, Y.Z. (Yufan Zhang), G.W. and Y.L.; formal analysis, X.L. and Y.Z. (Yufan Zhang); writing—original draft preparation, X.L.; writing—review and editing, X.L., L.Y. and Y.Z. (Yinghong Zhao); visualization, H.Q.; project administration, H.L. All authors have read and agreed to the published version of the manuscript.

Funding: This research was supported by the National Natural Science Foundation of China (No.52069004, No.42107189), Guizhou Provincial Science and Technology Projects (QKHJC-ZK [2021] YB293), and the Guizhou Province Graduate Research Fund (YJSKYJJ [2021] 064).

Institutional Review Board Statement: Not applicable.

Informed Consent Statement: Not applicable.

Data Availability Statement: Not applicable.

Acknowledgments: We are grateful to Chenrui Cao of Taiyuan University of Technology for his assistance in the experimental design and thesis writing of this study.

Conflicts of Interest: The authors declare no conflict of interest.

References

1. Jin, F.; An, X.; Shi, J.; Zhang, C. Study on rock-fill concrete dam. *J. Hydraul. Eng.* **2005**, *36*, 1347–1352.
2. Jia, J.; Lino, M.; Jin, F.; Zheng, C. The cemented material dam: A new, environmentally friendly type of dam. *Engineering* **2016**, *2*, 490–497. [[CrossRef](#)]
3. Jin, F.; Zhou, H.; An, X. Research on rock-filled concrete dam. *Int. J. Civ. Eng.* **2018**, *17*, 495–500. [[CrossRef](#)]
4. Xu, X.; Jin, F.; Zhou, H.; Bi, Z. Review on development and innovation of rock-filled concrete technology for dam construction. *J. China Three Gorges Univ. Nat. Sci.* **2022**, *44*, 1–11.
5. An, X.; Wu, Q.; Jin, F.; Huang, M.; Zhou, H.; Chen, C.; Liu, C. Rock-filled concrete, the new norm of SCC in hydraulic engineering in China. *Cem. Concr. Compos.* **2014**, *54*, 89–99. [[CrossRef](#)]
6. Liang, T.; Jin, F.; Huang, D.; Wang, G. On the elastic modulus of rock-filled concrete. *Constr. Build. Mater.* **2022**, *340*, 127819. [[CrossRef](#)]
7. He, S.; Zhu, Z.; Lv, M.; Wang, H. Experimental study on the creep behaviour of rock-filled concrete and self-compacting concrete. *Constr. Build. Mater.* **2018**, *186*, 53–61. [[CrossRef](#)]
8. Wei, H.; Zhang, G.; Sun, F.; Wang, M.; Li, W.; Xu, J. Experimental research on the properties of rock-filled concrete. *Appl. Sci.* **2019**, *9*, 3767. [[CrossRef](#)]
9. Li, Y.; Zhu, B.; Tang, X.; He, T.; Qiao, Z.; Wu, X.; Yang, L. Experimental study on mechanical properties of large-scale rock filled concrete specimen in Lvtang reservoir. *Water Resour. Plan. Des.* **2020**, *4*, 142–147.
10. Sim, J.; Yang, K.; Kim, H.; Choi, B. Size and shape effects on compressive strength of lightweight concrete. *Constr. Build. Mater.* **2013**, *38*, 854–864. [[CrossRef](#)]
11. Del Viso, J.; Carmona, J.; Ruiz, G. Shape and size effects on the compressive strength of high-strength concrete. *Cem. Concr. Res.* **2008**, *38*, 386–395. [[CrossRef](#)]

12. Zhuo, J.; Zhang, Y.; Ma, M.; Zhang, Y.; Zheng, Y. Uniaxial compression failure and size effect of recycled aggregate concrete based on meso-simulation analysis. *Materials* **2022**, *15*, 5710. [[CrossRef](#)]
13. Liu, B.; Zhang, J.; Du, Q.; Tu, J. A study of size effect for compression strength of rock. *Chin. J. Rock Mech. Eng.* **1998**, *166*, 611–614.
14. Li, K.; Yin, Z.; Han, D.; Fan, X.; Cao, R.; Lin, H. Size effect and anisotropy in a transversely isotropic rock under compressive conditions. *Rock Mech. Rock Eng.* **2021**, *54*, 4639–4662. [[CrossRef](#)]
15. Masoumi, H.; Douglas, K.; Russell, A. A bounding surface plasticity model for intact rock exhibiting size-dependent behaviour. *Rock Mech. Rock Eng.* **2016**, *49*, 47–62. [[CrossRef](#)]
16. Lloyd, D. Particle reinforced aluminium and magnesium matrix composites. *Int. Mater. Rev.* **1994**, *39*, 1–23. [[CrossRef](#)]
17. Yu, J.; Li, Y.; Zhou, H.; Xu, F. Influence of particle size on the dynamic behavior of PMMCs. *Acta Mater. Compos. Sin.* **2005**, *22*, 31–38.
18. Wang, Z.; Song, M.; Sun, C.; He, Y. Effects of particle size and distribution on the mechanical properties of SiC reinforced Al–Cu alloy composites. *Mater. Sci. Eng. A Struct. Mater. Prop. Microstruct. Process.* **2011**, *528*, 1131–1137. [[CrossRef](#)]
19. Lee, D. Fracture mechanical model for tensile strength of particle reinforced elastomeric composites. *Mech. Mater.* **2016**, *102*, 54–60. [[CrossRef](#)]
20. Tang, C. Numerical simulation of progressive rock failure and associated seismicity. *Int. J. Rock Mech. Min. Sci.* **1997**, *34*, 249–261. [[CrossRef](#)]
21. Xie, H.; Li, L.; Peng, R.; Ju, Y. Energy analysis and criteria for structural failure of rocks. *J. Rock Mech. Geotech. Eng.* **2009**, *1*, 11–20. [[CrossRef](#)]
22. Yang, T.; Liu, H.Y.; Tang, C. Scale effect in macroscopic permeability of jointed rock mass using a coupled stress-damage-flow method. *Eng. Geol.* **2017**, *228*, 121–136. [[CrossRef](#)]
23. Yang, T. Numerical Study Method of Seepage Characteristics in Rock Damage Process. Ph.D. Thesis, Dalian University of Technology, Dalian, China, 2019.
24. Jin, L.; Yu, W.; Du, X.; Yang, W. Meso-scale simulations of size effect on concrete dynamic splitting tensile strength: Influence of aggregate content and maximum aggregate size. *Eng. Fract. Mech.* **2020**, *230*, 106979. [[CrossRef](#)]
25. Weibull, W. The phenomenon of rupture in solids. *Proc. R. Swed. Inst. Eng. Res.* **1939**, *153*, 1–55.
26. Tang, C.; Tham, L.; Lee, P.; Tsui, Y.; Liu, H. Numerical studies of the influence of microstructure on rock failure in uniaxial compression—Part II: Constraint, slenderness and size effect. *Int. J. Rock Mech. Min. Sci.* **2000**, *37*, 571–583. [[CrossRef](#)]
27. Liang, Z.; Zhang, Y.; Tang, S.; Li, L.; Tang, C. Size effect of rock masses and associated representative element properties. *Chin. J. Rock Mech. Eng.* **2013**, *32*, 1157–1166.
28. Hu, G.; Ma, G. Size effect of parallel-joint spacing on uniaxial compressive strength of rock. *PLoS ONE* **2021**, *16*, e0257245. [[CrossRef](#)]
29. Wu, K.; Chen, B.; Yao, W. Study of the influence of aggregate size distribution on mechanical properties of concrete by acoustic emission technique. *Cem. Concr. Res.* **2001**, *31*, 919–923. [[CrossRef](#)]
30. Li, S.; Gao, D. Experimental research on the influence of coarse aggregate size on boulder concrete compressive strength. *Concrete* **2013**, *2*, 59–61.
31. Jin, L.; Yu, W.; Li, D.; Du, X. Numerical and theoretical investigation on the size effect of concrete compressive strength considering the maximum aggregate size. *Int. J. Mech. Sci.* **2021**, *192*, 106130. [[CrossRef](#)]
32. Hu, L.; Chen, X.; Dong, W. Mechanical properties and meso-scale failure mechanism of corundum pellet concrete with different aggregate sizes. *Concrete* **2021**, *10*, 70–75.

Disclaimer/Publisher’s Note: The statements, opinions and data contained in all publications are solely those of the individual author(s) and contributor(s) and not of MDPI and/or the editor(s). MDPI and/or the editor(s) disclaim responsibility for any injury to people or property resulting from any ideas, methods, instructions or products referred to in the content.